Journal of Applied Fluid Mechanics, Vol. 16, No. 12, pp. 2471-2482, 2023.
Available online at www.jafmonline.net, ISSN 1735-3572, EISSN 1735-3645.
https://doi.org/10.47176/jafm.16.12.1959

Application of an Open-Source OpenFoam for Fluid-Structure Interaction Analysis of the Horizontal-Axis Wind Turbine Blade

S. M. Belghoula[1†] and A. Benhamou[2]

[1] *Department of Hydraulics, Faculty of Civil Engineering, Hassiba Benbouali University of Chlef 02000, Algeria*
[2] *Laboratory of Mechanics and Energy (LME) Department of Mechanical Engineering, Faculty of Technology, Hassiba Benbouali university of Chlef 02000, Algeria*

†*Corresponding Author Email: m.belghoula@univ-chlef.dz*

ABSTRACT

This study investigates numerical simulation for fluid-structure interaction in wind turbine blades, emphasizing the influence of dimensionless numbers. Utilizing OpenFoam, the Navier-Stokes equation is accurately solved with the PISO algorithm, ensuring proper interface conditions. The icoFsiFoam solver is validated through dynamic testing, demonstrating its effectiveness. In contrast to the widely adopted Blade Element Momentum Theory (BEMT), our approach focuses on analyzing blade deformation and resonance phenomena, capturing intricate deformations and stress concentrations. Our investigation explores the impact of reduced velocity on blade behavior across a range of 0.105 to 0.145, while consistently maintaining crucial dimensionless numbers such as Reynolds number (Re = 10^6), Froude number (Fr = 4.93), and Cauchy number (C_y=10^{-5}). The outcomes of this study significantly contribute to the understanding of fluid-structure interaction in wind turbine blades. By examining the oscillatory behavior of the blades, we observe trends similar to those predicted by BEMT. However our approach surpasses BEMT by providing additional insights into stress concentrations and deformation modes. This advancement enables superior performance optimization and facilitates advanced blade analysis. The implications of our research are paramount for optimizing blade design and performance under varying reduced velocities. By incorporating the findings of this study, blade designers can make well-informed decisions to enhance the efficiency and durability of wind turbine technologies. The presented methodology and results provide a comprehensive investigation into the fluid-structure interaction of wind turbine blades, highlighting the importance of dimensionless numbers and their influence on blade behavior. Overall, this study offers valuable insights for improving wind turbine design and performance.

Article History

Received April 24, 2023
Revised July 18, 2023
Accepted July 26, 2023
Available online October 8, 2023

Keywords:

Fluid-structure interaction
Wind blade turbine
Dimensionless analysis
Numerical simulation
OpenFoam

1. INTRODUCTION

In recent years, significant advancements have been made in the numerical simulation of multi-physics problems, driven by the progress in computer resources, modeling techniques, and mathematical and numerical analysis in fluid mechanics and solid mechanics (Takizawa et al., 2012; Cheng et al., 2017). In the field of wind turbine aerodynamics, various methods have been employed for predicting aerodynamic performance, such as the Blade Element Momentum (BEM) theory (Mdouki, 2020; Moghimi & Motawej, 2020; Adjiri et al., 2023), vortex theory (Lee & Kwon, 2019; Schaffarczyk & Schaffarczyk, 2014; Agbormbai, 2021), and the active disk method (Năstase, 2021).

While simplified approaches like BEM assume independent blade elements, the vortex method offers more accurate solutions under specific conditions but requires greater computational resources.

The most accurate method, Computational Fluid Dynamics (CFD), is widely recognized but comes with higher computational costs (Casillas Farfán et al., 2022; Adjiri et al., 2023; Bouhelal et al., 2023).

Researchers extensively employ CFD-CSD methods to enhance aerodynamic predictions, surpassing the limitations of BEM models.

Nomenclature

C	damping coefficient	Re	Reynolds number
C_L	lift coefficient	St	Strouhal number
C_y	Cauchy number	**U**	fluid velocity
D	reduced displacement	Ur	reduced velocity
$\mathbf{e_z}$	unit vector in z direction	**Greek symbols**	
f	beam vibration frequency	$\bar{\varepsilon}$	strain tensor
F_0	amplitude force	η_s	corresponding damping coefficient
Fr	Froude number	μ_f	dynamic viscosity of the fluid
g	gravitational acceleration	ξ	solid displacement vector
I	area moment of inertia	ρ_f	fluid density
$\bar{I}$	Kronecker tensor	ρ_s	solid density
K	spring coefficients	$\bar{\sigma}$	Cauchy constraint tensor
L	characteristic length	σ_{eq}	equivalent stress
p	fluid pressure		

With the increasing focus on aeroelasticity studies in wind turbine technology, it is crucial to consider blade deformation in predicting wind turbine performance. Recent studies have utilized 3D CFD-CSD simulations on the National Renewable Energy Laboratory (NREL) 5 MW rotor (Hsu & Bazilevs, 2012; Sayed et al., 2019; Tang et al., 2019; Bouhelal et al., 2023).

In this study, we investigate the influence of wind on blade behavior and vice versa using the fluid-structure interaction (FSI) method to refine wind turbine blade performance predictions. FSI problems commonly encountered in industrial applications involve the interaction between fluid and solid subdomains, with a focus on studying the deformation of solid structures in the presence of fluids (Degroote, 2013; Dahmane et al., 2016; Sjah & Vincens, 2017). To address the limitations of Lagrangian or Eulerian descriptions, researchers have developed the Arbitrary Lagrangian-Eulerian (ALE) method, which combines the advantages of both approaches and satisfies the Geometric Conservation Law (GCL) (Scovazzi & López Ortega, 2012).

The behavior of a solid structure submerged in a fluid can be strongly influenced by the fluid's action, such as the lift force generated by the flow on a turbine blade, which can induce blade motion. However, these flow-induced vibrations can also potentially damage the structure. Therefore, in this study, we numerically simulate the fluid-structure interaction of a turbine blade and investigate the influence of dimensionless numbers, specifically reduced speed, on the blade's behavior.

We present three simulations, as summarized in Table 1 below, and validate the dynamics by considering dynamic equations (Mohebbi & Hashemi, 2017; Moghimi & Motawej, 2020). In our approach, we conduct dimensional analysis for both the fluid and solid domains to derive dimensionless numbers such as Reynolds number (Re), Froude number (Fr), reduced velocity (Ur), and Cauchy number (Cy). By varying the reduced speed while keeping other dimensionless numbers constant, we assess the impact on the turbine blade's behavior.

We utilize the open-source solver icoFsiFoam integrated into the OpenFOAM software for this study.

Table 1 Summary table of our simulation study.

Simulation:	Ur	Re	Fr	C_y
	0.105	10^6	4.93	10^{-5}
b	0.125	10^6	4.93	10^{-5}
c	0.145	10^6	4.93	10^{-5}

Before applying the icoFsiFoam solver to the case study, we perform validation through a theoretical study on the vibration of a cylindrical beam (Sabino et al., 2020; Ebrahimi et al., 2021; Wu et al., 2023).

In summary, our study explores the fluid-structure interaction of a turbine blade, considering the influence of dimensionless numbers, particularly reduced speed. We refine predictions of wind turbine blade performance by employing the FSI method and investigate the impact of reduced speed on the blade's behavior. We vary the reduced velocities, Ur, with values set to 0.105, 0.125, and 0.145, while keeping all other dimensionless numbers, including the Reynolds number (Re = 10^6), Froude number (Fr = 4.93), and Cauchy number (C_y=10^{-5}), constant.

By conducting this comprehensive investigation of fluid-structure interaction in wind turbine blades, our study offers a realistic and complementary perspective to the widely adopted Blade Element Momentum Theory (BEMT). While BEMT focuses on analyzing blade deformation and potential resonance phenomena, our approach goes beyond by capturing intricate blade deformations, providing additional insights into stress concentrations and deformation modes.

This advancement enables superior performance optimization and facilitates advanced blade analysis.

The primary objective of this investigation is to explore the impact of reduced velocity on wind turbine blade behavior, covering a comprehensive range from 0.105 to 0.145. Additionally, other crucial dimensionless numbers, such as the Reynolds number (Re = 10^6), Froude number (Fr = 4.93), and Cauchy number (C_y=10^{-5}), are consistently maintained throughout the study.

The presented methodology and results significantly contribute to the understanding of fluid-structure interaction in wind turbine blades. The implications of this research are paramount for optimizing blade design and performance under varying reduced velocities. By incorporating the findings of this study, blade designers can make well-informed decisions to enhance the efficiency and durability of wind turbine technologies.

2. GOVERNING EQUATIONS AND SOLUTION METHOD

In this section, the mathematical and numerical tools used in our study are presented. The equations of continuity and motion for incompressible fluids, as well as the conservation equation of momentum for the solid medium and the interface equation, are described. The approach is then validated through a dynamic simulation of the vibration of a cylindrical beam.

2.1 Conservation and Interface Equations

A homogeneous, incompressible Newtonian fluid with constant and uniform viscosity is considered. The conservation of mass is expressed as follows:

$$\boldsymbol{\nabla}.\mathbf{U}=0. \tag{1}$$

The motion equation is represented by:

$$\rho_f \frac{d\mathbf{U}}{dt}=-\rho_f g\mathbf{e_z} - \boldsymbol{\nabla}p+\mu_f \Delta\mathbf{U}. \tag{2}$$

Where, $\mathbf{U}$, ρ_f and p represents fluid velocity field, fluid density and pressure respectively. In the solid medium, it is assumed that the material is elastic and isotropic. The relationship between the displacement vector and strain tensor is governed by the conservation of the quality of motion.

$$\rho_s \frac{\partial^2 \boldsymbol{\xi}}{\partial t^2}=-\rho_s g\mathbf{e_z}+\boldsymbol{\nabla}.\bar{\sigma}. \tag{3}$$

In which, ξ, ρ_s and $\bar{\sigma}$ are respectively displacement vector, solid density and Cauchy constraint. With the law of elastic behavior:

$$\bar{\varepsilon}=\frac{1+\nu}{E}\bar{\sigma} - \frac{\nu}{E}\mathrm{Tr}(\bar{\sigma})\bar{I}. \tag{4}$$

And:

$$\bar{\varepsilon}=\frac{1}{2}\left(\boldsymbol{\nabla}\boldsymbol{\xi}^t + \boldsymbol{\nabla}\boldsymbol{\xi}\right), \tag{5}$$

$\bar{\mathcal{E}}$, $\bar{I}$ are the strain and Kronecker tensors respectively. In equation (4), ν represent the Poisson's ratio and E the Young's modulus.

The equivalent stress is given by:

$$\sigma_{eq}=\sqrt{\frac{(\sigma_{xx}-\sigma_{yy})^2+(\sigma_{yy}-\sigma_{zz})^2+(\sigma_{zz}-\sigma_{xx})^2}{2}}. \tag{6}$$

At the interface, the displacement velocity is defined by:

$$\mathbf{U}=\frac{\partial \boldsymbol{\xi}}{\partial t}. \tag{7}$$

And:

$$\left[-p\bar{I}+2\mu_f\bar{d}\right].\mathbf{n}=\bar{\sigma}.\mathbf{n}, \tag{8}$$

whence

$$\bar{d}=\frac{1}{2}\left(\boldsymbol{\nabla}\mathbf{U}^t+\boldsymbol{\nabla}\mathbf{U}\right). \tag{9}$$

The normal of the interface $\mathbf{n}$ is directed from solid towards fluid. The following variables are used to render equations dimensionless:

$$x^*=\frac{x}{L},\ t^*=t\frac{\sqrt{E/\rho_s}}{L},\ \mathbf{U}^*=\frac{\mathbf{U}}{U_0},\ p^*=\frac{p}{\rho_f U_0^2},$$

$$U_r=\frac{U_0}{\sqrt{E/\rho_s}},\ \boldsymbol{\xi}^*=\frac{\boldsymbol{\xi}}{\xi_0},\ \sigma^*=\frac{\sigma}{E}. \tag{10}$$

U_0 , U_r and L are called respectively reference velocity, reduced velocity and characteristic length. With these changes, the fluid equation is obtained.

$$\boldsymbol{\nabla}.\mathbf{U}^*=0. \tag{11}$$

$$\frac{1}{U_r}\frac{d\mathbf{U}^*}{dt^*}=\frac{-1}{Fr^2}\mathbf{e_z} - \boldsymbol{\nabla}p^* + \frac{1}{Re}\Delta\mathbf{U}^*. \tag{12}$$

Where Fr and Re are the Froude and Reynolds numbers, respectively. For the solid equations, the following equations are obtained:

$$\mathcal{D}\frac{\partial^2 \boldsymbol{\xi}^*}{\partial t^{*2}}=\frac{-Ur^2}{Fr^2}\mathbf{e_z}+\nabla.\bar{\sigma}^*, \tag{13}$$

$$\frac{\mathcal{D}}{2}\left(\nabla^t\bar{\boldsymbol{\varepsilon}}^*+\bar{\boldsymbol{\varepsilon}}^*\right)=(1+\nu)\bar{\sigma}^* - \nu T_r\left(\bar{\sigma}^*\right)\bar{I}. \tag{14}$$

The dynamic condition can be written as:

$$C_y\left[-p^*\bar{I}+\frac{2}{Re}\bar{d}^*\right].\mathbf{n}=\bar{\sigma}^*.\mathbf{n}. \tag{15}$$

In equations (13-14), $\mathcal{D}$ and C_y represents, reduced displacement, Cauchy number respectively:

$$\mathcal{D}=\frac{\xi_0}{L},\ C_y=\frac{\rho^0_{f}U_0^2}{E}. \tag{16}$$

2.2 Fluid-Structure Coupling

In our work, mechanical fluid-structure interactions are of interest, i.e., the exchanges between a fluid domain and a structure domain that are satisfied by the following conditions (Yang et al., 2022):

- fluid and structure exchange mechanical energy,
- there is no mass transfer between the fluid and the structure,
- the phenomena involved are multi-physical.

FSI problems falling within this framework can be classified according to different criteria: (de Langre, 2001):

- stationary flow,
- aeroelasticity (pseudo-static and quasi-static),
- strong coupling.

For the case of weak coupling, the exchange of energy between the fluid and the solid is negligible, and it is therefore sufficient to solve the two domains independently without taking into account the reciprocal influence of the fluid and solid media. On the other hand,

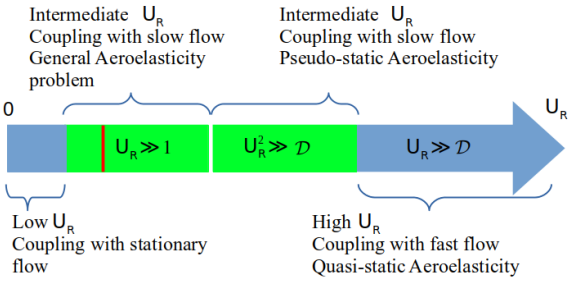

Fig. 1 Classification of FSI problems according to reduced velocity value

there are problems for which the exchange of energy is important, where the fluid exerts a pressure on the structure causing its deformation. In this case, it is necessary to represent the feedback existing between the fluid and solid media, and the coupling used is strong.

The Fig. 1 summarizes the influence of the criteria on the classification of FSI problems.

2.3 Formulation of Lift and Drag Forces

Significant contributions to the field of wind turbine design have been made by Panjwani et al. (2014) through their research on the development of wind farm design tools based on the actuator line/actuator disk concept in the OpenFoam architecture. In the formulation of lift and drag forces in wind turbines, valuable insights have been provided by their work.

The lift effect, utilized by wind turbine blades (see Fig. 2), is generated through the airflow around their profile. This effect is caused by the acceleration of the airflow over the upper surface (extrados) compared to the lower surface (intrados) of the blade, resulting in a region of reduced pressure over the extrados.

The longer distance that the air has to travel over the extrados compared to the intrados can be attributed to the higher air speed observed over the extrados. To ensure a consistent airflow at the front and rear of the blade, the air is accordingly accelerated. As a consequence, a perpendicular lift force is exerted on the blade with respect to the wind direction.

The lift force is calculated by the following formula:

$$F_z=\frac{1}{2}\rho v^2 A C_z \quad (17)$$

Conversely, the drag force, which opposes the forward motion of the blade, is determined by the air resistance. The surface area exposed to the airflow direction increases the air resistance. The drag force is experienced by the blade in the same direction as the wind, necessitating its minimization. The calculation of the drag force is as follows:

$$F_x=\frac{1}{2}\rho v^2 A C_x \quad (18)$$

In equations (1) and (2), ρ, v, C_x, and C_z are respectively embodied by the air density, relative velocity of the wind with respect to the blade, drag and lift coefficients. A in the equations is embodied by the area of the blade, provided by:

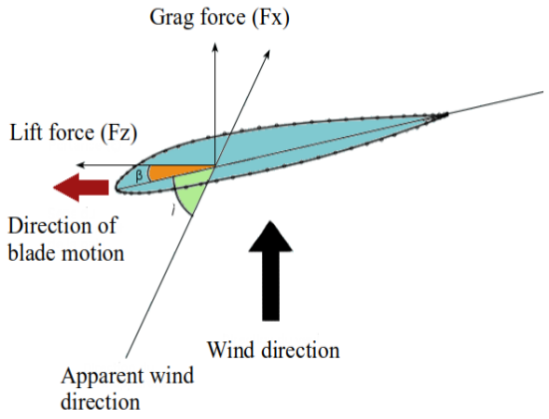

Fig. 2 Cross sectional view of the blade airfoil

$$A=L\times C \quad (19)$$

Where, L and C are respectively represented by the length and chord of the blade. The research conducted by Panjwani et al. (2014), along with these formulations, contributes to the understanding and optimization of wind turbine performance and design.

3. NUMERICAL MODELING

In this section, the simulation results obtained in the solid domain using the OpenFoam source-code are presented. The icoFsiFoam solver enabled us to solve, in a non-stationary regime, the equations of motion in the fluid medium as well as the conservation of momentum equation in the solid medium. The blade structure used in our study is a taper less blade that incorporates a National Advisory Committee for Aeronautics (NACA) 4412 airfoil (Lololau et al., 2021). Results were generated using an Intel dual quad core 3.06 GHz CPU having 1.5 GB RAM and running on the Linux operating system. The Table 1 below summarizes all the simulation data.

3.1 Computational Grid and Boundary Conditions

The wind turbine blade is positioned at a distance of $10 \times C_0$ from the inlet, $5 \times C_0$ from the walls, and the outlet is located $30 \times C_0$ away from the blade. Here, C_0 represents the characteristic length, which is the maximum length of the chord. The domain of the rectangular parallelepiped is there- fore $(40 \times 10 \times 10)$ C_0^3 (refer to Fig. 3). The reduced velocities, Ur, were only varied, with values set to 0.105, 0.125, and 0.145. All other dimensionless numbers, such as Reynolds number ($Re = 10^6$), Froude number ($Fr = 4.93$), and Cauchy number ($C_y=10^{-5}$), were held constant.

In the fluid domain, a regular grid of $(40 \times 40 \times 40)$ cells was chosen in the three directions with hexahedral shapes, while in the solid domain, a tetrahedron mesh type was chosen. The imposed boundary conditions in the fluid domain are:

- **Inlet:** velocity imposed and $\frac{\partial p}{\partial x}=0$,
- **Outlet:** pressure imposed and $\frac{\partial U}{\partial x}=0$,

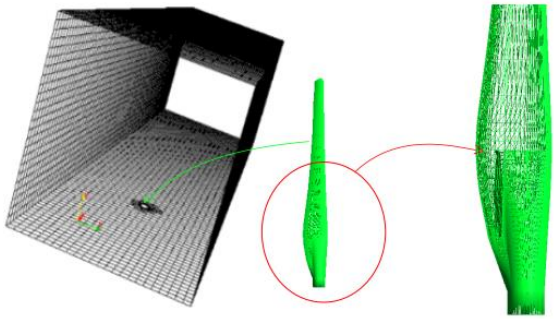

Fig. 3 Different types of mesh used in fluid (left) and solid (right) domain

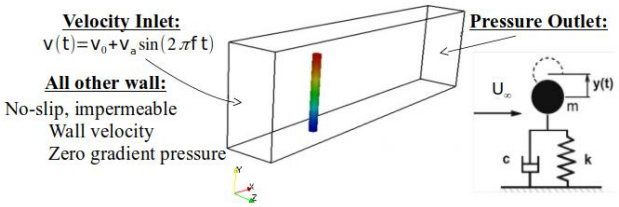

Fig. 4 Equivalent system (right) and boundary conditions imposed on the computational domain (left)

- **Walls:** no-slip boundary condition for velocity and $\frac{\partial p}{\partial x}=0$.

At the fluid-structure interface, the dynamic conditions were imposed as follows:

- $\mathbf{U}=\frac{\partial \xi}{\partial t}$ and $\left[-p\bar{I}+2\mu_f\bar{d}\right].\mathbf{n}=\bar{\sigma}.\mathbf{n}$.

3.2 Dynamic Validation of a Cylindrical Beam

In this part, the dynamic validation of the cylindrical beam vibration is developed, inspired by the one degree of freedom (DOF) model (Mohebbi & Hashemi, 2017) with a diameter D = 0.2m and height H = 2m having the following mechanical properties, Young Modulus E = 6.6219 $\times 10^7$ kg/m.s², Poisson's ration ν = 0.3 and the density ρ_s= 1000 kg/m³. Under these conditions the natural frequency of material constituting the beam is f = 5Hz:

$$f=\frac{1}{2\pi}\sqrt{\frac{12EI^3}{\rho_s AH^4}}, \tag{20}$$

I is the area moment of inertia and A is a cross section of the beam. The domain of the fluid is characterized by a rectangular parallelepiped of size $(8\times2.5\times1.2)m^3$, see Fig. 4 (right). A code validation study is presented (Soti & De, 2020) where they studied the effect of fluid confinement on power extraction efficiency of the cylinder.

The Reynolds number as well as the density ratio is fixed to Re=400 and $\frac{\rho_s}{\rho_f}=100$ respectively. The Fig. 4 (left) represents the equivalent scheme of the system; the characteristic's equation of such system is described under the following formula:

$$y''+Cy'+Ky=F_0(\sin(2\pi ft)-\cos(2\pi ft)). \tag{21}$$

Were c and k are respectively, the damping and spring coefficients given by many authors (Gopalkrishnan, 1993; Hover et al., 1998, Sarpkaya, 2004):

$$C=4\eta_s\pi fk=4\pi^2f^2. \tag{22}$$

In which η_s is the damping coefficient. F_0 is the amplitude force given by the formula:

$$F_0=\frac{4C_LU_0^2}{2D\left(1+\frac{\rho_s}{\rho_f}\right)}. \tag{23}$$

With C_L is the lift coefficient. The Fig. 5 shows clearly the validity of the **icoFsiFoam** solver for our study, the latter is translated by a good agreement between the numerical and theoretical results.

The amplitude of the established response of thisoscillation to a harmonic forcing is (Gopalkrishnan, 1993; Hover et al., 1998, Sarpkaya, 2004):

$$|y|=\frac{1}{2}\rho_fU_\infty^2DC_L\frac{1}{k}\frac{1}{\left[\left(1-(\omega_F/\omega)^2\right)^2+(c\omega_F/k)^2\right]^{1/2}} \tag{24}$$

With $\omega^2=K$ and $\omega_F=\frac{2\pi SU_\infty}{D}$, however the amplitude evolves with the flow velocity. The resonance is reached at reduced speed $U_R=\frac{1}{St}$, where St is the Strouhal number. The frequency of the oscillation vortex shedding coincides with the frequency of the oscillator.

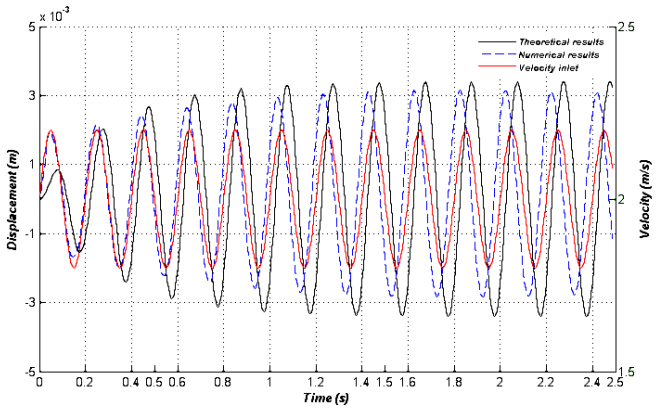

Fig. 5 Comparison between the numerical (--) and theoretical results (—) for a given velocity profile(—)

The Fig. 5 presented below demonstrates a good conformity between these two aspects. However, a slight deviation can be observed, which can be attributed to factors such as approximations present in the theoretical models or numerical errors associated with the resolution of mathematical equations. Despite this slight deviation, the numerical and theoretical results remain overall consistent, indicating a good alignment between the two approaches. This conformity between the theoretical and numerical frequencies strengthens the validity of the employed models and supports the effectiveness of the numerical approach adopted for problem resolution.

4. RESULTS AND DISCUSSION

In this section, we focus solely on the deformation of the blade, and therefore, results related to the fluid, such as velocity and pressure fields, have been omitted. Our primary goal is to analyze the behavior of the blade, including its deformation and possible resonance phenomena. The analysis of the figures presented in this section led us to the conclusion that the blade's response over time resembles that of a spring-damper system, as shown in Fig. 6 (left) and Fig. 6 (right). These figures demonstrate that, for the two orthogonal directions, the oscillations according to the reduced speeds are in phase. Furthermore, the damping of the blade is more pronounced at lower reduced speeds. The stationary regime is eventually reached, and the displacements along the two axes stabilize. As the focus of this work is solely on the blade's deformation, the results related to the fluid, such as velocity and pressure fields, have not been presented. To ensure stability in our calculations, a courant number (CFL) of 0.2 was employed during the explicitly discretized simulations. For the implicit discretization, the speed criterion for mesh displacement was reduced to stabilize the simulations. In addition to the Courant number stability criterion, an adaptive time step criterion was also employed.

Most authors (Apsley & Stansby, 2020; Mannion et al., 2020) utilize the Blade Element Momentum Theory (BEMT) to model the interaction between the fluid and the wind turbine blade. Figures 7 (left) and 7 (right) depict the drag force and lift force, respectively, obtained from our numerical simulations. It is evident that these forces stabilize and reach constant values along the orthogonal axes after a certain point, indicating the attainment of a steady state.

To validate our findings and provide a comprehensive analysis of the wind turbine blade's behavior, we developed an alternative approach that deviates from the conventional use of the Blade Element Momentum Theory (BEMT). While BEMT is commonly employed to model the interaction between the fluid and wind turbine blades, we sought to explore a different methodology that could offer additional insights and validate our results. Our approach, which focuses on analyzing the blade's deformation and potential resonance phenomena, offers a novel perspective. By examining the oscillatory behavior of the blade, as

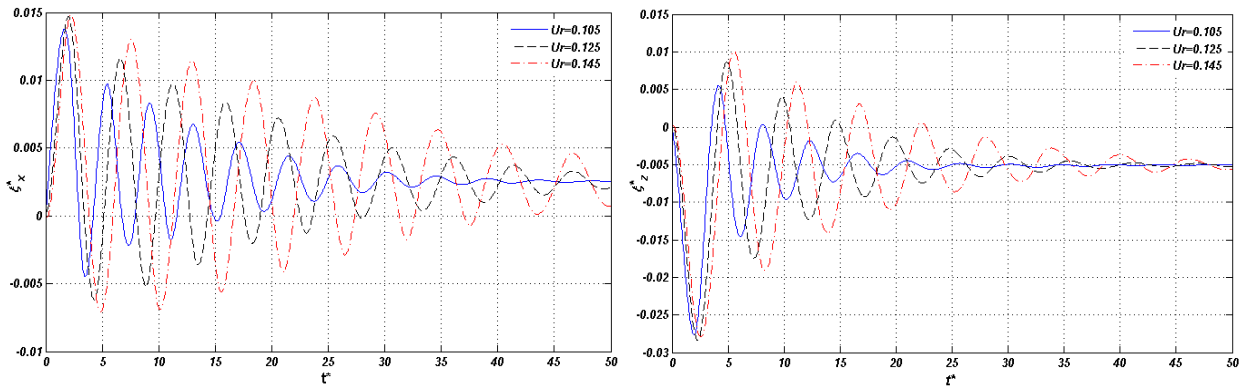

Fig. 6 Longitudinal (left) and transverse (right) dimensionless displacements of a marker point placed on top of the blade at various reduced velocities

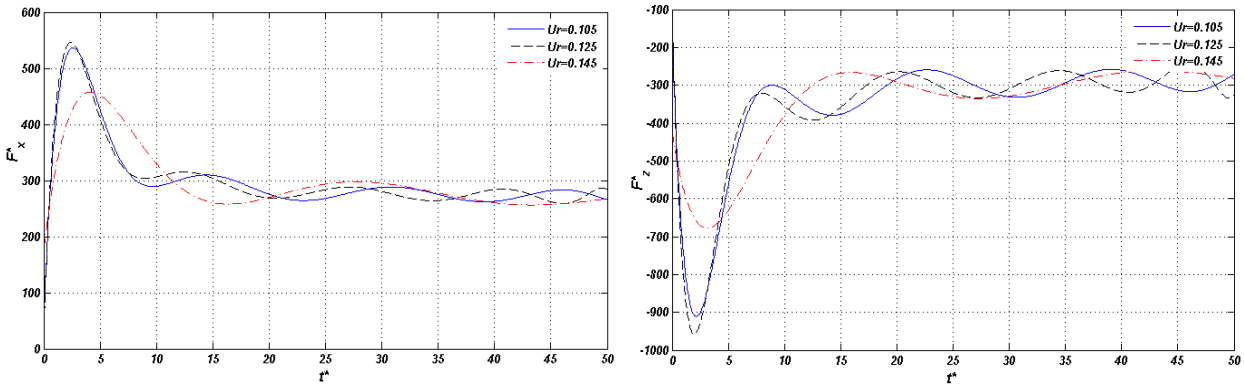

Fig. 7 Equivalent Drag (left) and Lift (right) dimensionless forces applied on the blade for different Reduced Velocities

depicted in Fig. 6 (left) and Fig. 6 (right), we observed consistent trends and characteristics that resemble those predicted by BEMT. Although a direct comparison with BEMT was not conducted in this study, our approach provides a valuable alternative that showcases the effectiveness of our numerical simulations in capturing the dynamic response of the blade. Future work should include a more in-depth comparison between our approach and BEMT to further validate our findings and establish the merits of our methodology.

Our approach captures detailed blade deformation dynamics, surpassing traditional methods like BEMT. It provides insights into stress concentrations and mode shapes, improving performance optimization. By integrating simulations and focusing on deformation and resonance, our approach complements BEMT for advanced blade analysis. Further research should validate and refine our approach through experiments and direct BEMT comparisons.

Figures 8.a, 8.b, and 8.c illustrate the adimensional distribution of the displacement field on the extrados side of the blade, which is attributed to the pressure forces exerted by the surrounding fluid. These figures present the modulus of the dimensionless displacement field for all the simulations described in table 1. From these results, it is apparent that the blade deformation exhibits a linear dependency on the reduced speed. In other words, an increase in the reduced speed corresponds to an increase in both the blade displacement and its deformation.

Due to computational constraints, our analysis was limited to a narrow range of reduced speeds. Initially, the vibratory movement exhibited significant amplitude but gradually diminished over time. The duration required for damping the vibratory motion and reaching a steady state primarily depends on the reduced velocity, Ur. While our primary focus was on investigating the blade's behavior by varying the reduced speed, it is worth noting that considering variations in other dimensionless numbers, such as Reynolds number (Re) and Cauchy number (C_y), would also be of importance.

An interesting observation can be made regarding the evolution of the point located at the top of the blade in a plane parallel to the flow (see Fig. 9). For the three values of reduced speed, the trajectories of the marker form concentric ellipses that gradually decrease in size until reaching equilibrium.

At this equilibrium point, the fluid flow tends towards a stationary regime, where all physical parameters of the fluid, such as pressure and velocity, no longer change over time. In such cases, the system is considered stable.

Our results also indicate that the blade displacement is relatively small, which can be attributed to the low Reynolds number ($Re = 10^6$) and, consequently, the low inertial forces. To prevent any instability phenomena, such as blade flutter, dimensionless numbers related to both the fluid and the blade material (Re, Fr and C_y) were carefully chosen, ensuring the optimal operation of the wind turbine.

The distribution of the dimensionless equivalent stress field along the intrados side of the wind turbine blade over time is depicted in Figs 10.a, 10.b, and 10.c.

By observing these results, valuable insights can be gained into the behavior of the wind turbine blade during fluid-structure interaction and the influence of different forces.

Initially, the stress is subjected to pressure forces from the early moments of the simulations, after which it stabilizes, indicating the blade's stability. The reduction in stress over time can be explained by the phenomenon of stress redistribution along the blade. Initially, higher stress levels are experienced in certain areas of the blade due to factors such as geometry, load conditions, and material properties. However, as time progresses, the stresses redistribute more uniformly, resulting in a decrease in the overall equivalent stress.

This process of stress redistribution is a typical outcome of the cyclic loads to which the blade is exposed.

Furthermore, these findings have implications for optimizing wind turbine blade design and enhancing their resistance to cyclic loads. Understanding stress redistribution helps identify highly stressed areas and take appropriate measures to strengthen them, prolonging the lifespan of the blades and optimizing their performance.

Moreover, analyzing stress redistribution provides insights into potential failure mechanisms of wind turbine blades, crucial for ensuring the safety and reliability of wind energy installations.

The obtained results can contribute to the development of new design and manufacturing techniques for stronger and more durable blades.

The analysis of the distribution of equivalent stresses along the wind turbine blade provides valuable insights into its behavior during fluid-structure interaction. This in-depth understanding allows for design optimization, improved resistance to cyclic loads, and ensuring the performance and durability of wind turbine blades under real operational conditions.

It is worth noting that this decrease in stress over time can also be influenced by other factors specific to the simulation model, such as boundary conditions and blade characteristics. Understanding and interpreting this stress redistribution can provide valuable insights for optimizing the design and ensuring the durability of horizontal-axis wind turbine blades. By analyzing the distribution of equivalent stresses over time and at different reduced velocities along the wind turbine blade, a better understanding of the impact of different forces, such as random forces, fluid-structure forces, and fluid-elastic forces, can be obtained. This information is crucial for optimizing the resistance and behavior of the blade during fluid-structure interaction, ultimately contributing to the development of more efficient and durable wind turbine technologies.

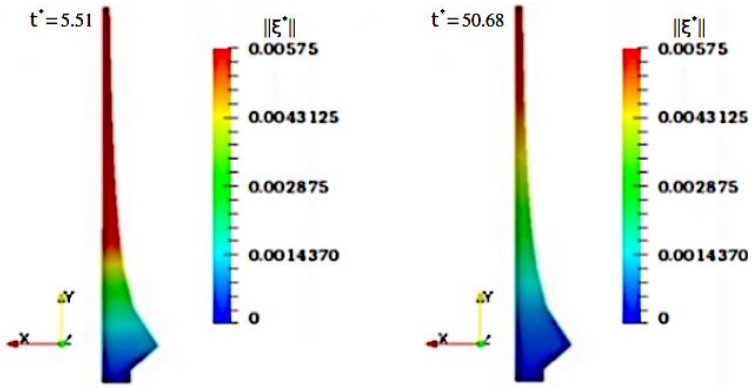

Fig. 8a Dimensionless displacement field along the extrados side of blade for: Ur = 0.105, Re = 10^6, Fr = 4.93 and $C_y = 10^{-5}$

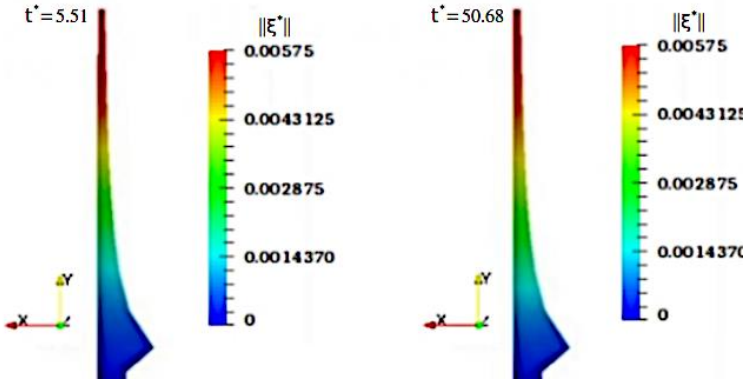

Fig. 8b Dimensionless displacement field along the extrados side of blade for: Ur = 0.125, Re = 10^6, Fr = 4.93 and $C_y = 10^{-5}$

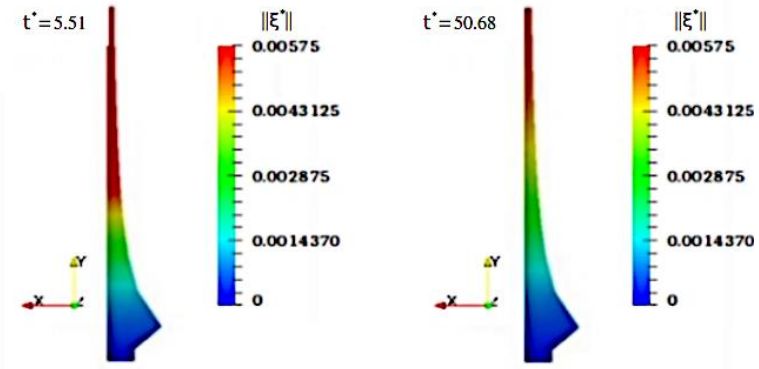

Fig. 8c Dimensionless displacement field along the extrados side of blade for: Ur = 0.145, Re = 10^6, Fr = 4.93 and $C_y = 10^{-5}$

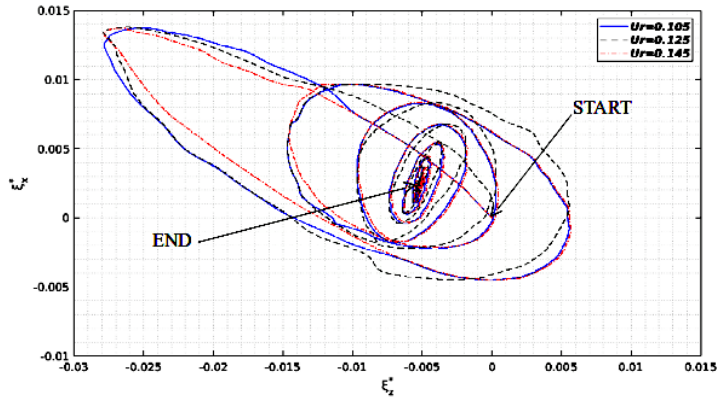

Fig. 9 Marker's Trajectory positioned at the top of the blade for Ur = 0.105, Ur = 0.125 and Ur = 0.145

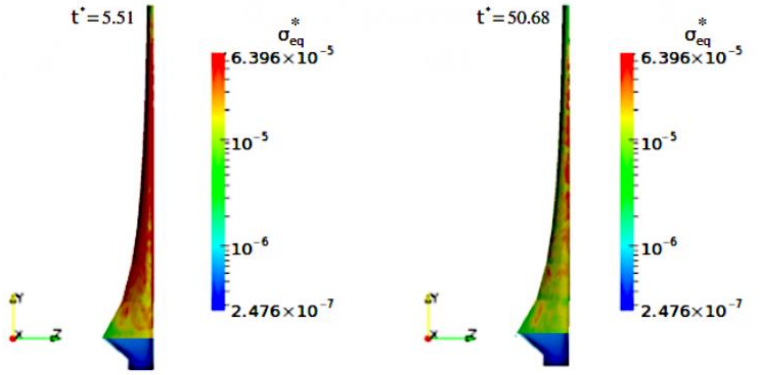

Fig. 10a Dimensionless equivalent stress field along the intrados side of blade for: Ur = 0.105, Re = 10^6, Fr = 4.93 and $C_y = 10^{-5}$

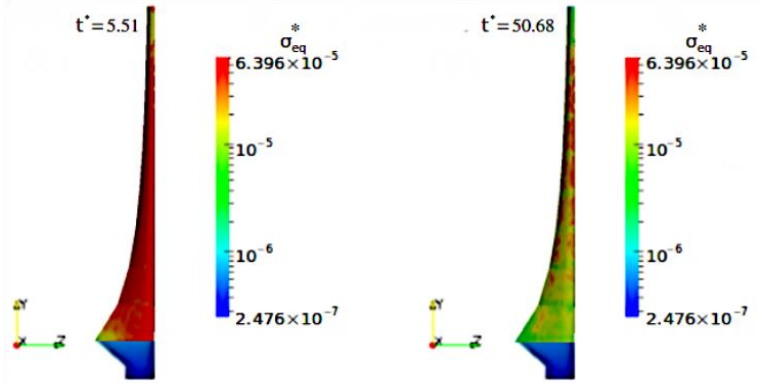

Fig. 10b Dimensionless equivalent stress field along the intrados side of blade for: Ur = 0.125, Re = 10^6, Fr = 4.93 and $C_y = 10^{-5}$

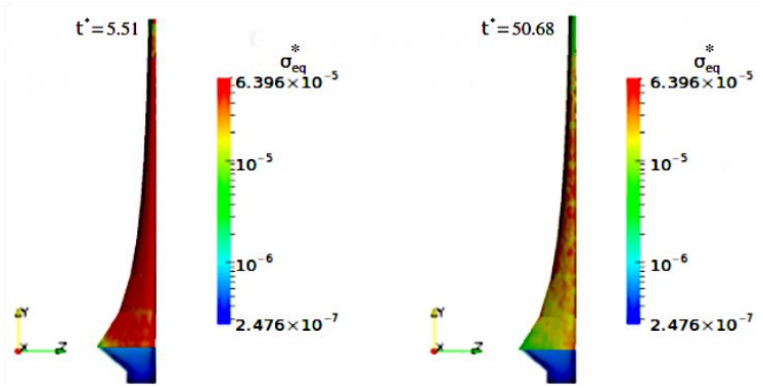

Fig. 10c Dimensionless equivalent stress field along the intrados side of blade for: Ur = 0.145, Re = 10^6, Fr = 4.93 and $C_y = 10^{-5}$

5. CONCLUSION

In this study, we have provided significant insights into the behavior of wind turbine blades under fluid-structure interaction. The analysis of blade displacement has revealed a noteworthy spring-damper system-like response, with prominent in-phase oscillations along the two orthogonal directions. Furthermore, we have observed that blade damping becomes increasingly substantial as the reduced speed decreases, eventually leading to significant stabilization of displacements along both axes. To ensure the stability of our simulations, meticulous discretization methods and criteria have been employed.

Additionally, we have presented and analyzed the deformations of the blade over time, influenced by the pressure forces exerted by the surrounding fluid. The modulus of the dimensionless displacement field has demonstrated a strong linear relationship with the reduced speed, indicating that higher reduced speeds

result in considerable blade displacement and deformation. However, due to computational limitations, our study has focused on a limited range of reduced speeds.

In comparison to the widely used Blade Element Momentum Theory (BEMT) employed by most authors, our numerical simulations have revealed the equivalent drag and lift forces acting on the wind turbine blade. Our figures strikingly illustrate that these forces stabilize and reach constant values after a certain period, indicating the attainment of a steady state.

The initially substantial amplitude of vibratory movement gradually diminishes over time, reaching a stationary state primarily dependent on the reduced velocity. While our study specifically investigated the behavior of the blade by varying the reduced speed, it is evident that further consideration of other essential dimensionless numbers, such as Reynolds and Cauchy numbers, would provide a more comprehensive understanding of the fluid-structure interaction phenomenon.

Through the analysis of the distribution of equivalent stresses over time and at different reduced velocities along the wind turbine blade, we gain a profound understanding of the impact of various forces, including random forces, fluid-structure forces, and fluid-elastic forces. This knowledge is crucial for optimizing the resistance and behavior of the blade during fluid-structure interaction, ultimately contributing to the development of highly efficient and exceptionally durable wind turbine technologies.

In summary, our findings emphasize the remarkable significance of dimensionless numbers in comprehending the behavior of fluid-structure interaction in horizontal-axis wind turbine blades. The validated numerical simulations provide invaluable insights for blade designers to optimize their designs while considering different reduced velocities, thus ensuring optimal performance. We strongly emphasize the influence of dimensionless numbers on blade behavior, contributing to the advancement of knowledge in this field. The constant values for the Reynolds number ($Re = 10^6$), Froude number ($Fr = 4.93$), and Cauchy number ($C_y=10^{-5}$) have been maintained throughout this study. These findings serve as a precious resource for future research endeavors in the field of fluid-structure interaction in wind turbines.

Moreover, we have introduced an alternative approach that deviates from the conventional use of the Blade Element Momentum Theory (BEMT) to further validate and comprehensively analyze the wind turbine blade's behavior. While BEMT is commonly employed to model the interaction between the fluid and wind turbine blades, our novel approach, which focuses on meticulously analyzing the blade's deformation and potential resonance phenomena, offers a distinct and valuable perspective. By examining the consistent trends and characteristics in the blade's oscillatory behavior, as depicted in prominent figures, we observed patterns that resemble and validate those predicted by BEMT. Although a direct comparison with BEMT was not conducted in this study, our approach provides a significant alternative that showcases the effectiveness of our numerical simulations in capturing the dynamic response of the blade. Future work should include a more in-depth comparison between our approach and BEMT to further validate our findings and establish the merits of our methodology.

Our approach captures intricate blade deformation dynamics, surpassing traditional methods like BEMT. It provides profound insights into stress concentrations and mode shapes, significantly enhancing performance optimization. By integrating simulations and focusing on deformation and resonance, our approach complements BEMT for advanced blade analysis. Further research should meticulously validate and refine our approach through experiments and direct BEMT comparisons.

CONFLICT OF INTEREST

The authors declare that they have no competing financial interests or personal relationships that could have influenced the work presented in this paper. This statement is provided in full compliance with the policies of the Journal of Applied Fluid Mechanics, and the authors take full responsibility for its accuracy.

AUTHOR CONTRIBUTION

Both authors, S. M. Belghoula and A. Benhamou, actively contributed to the analysis and interpretation of the results. S. M. Belghoula, as the lead author, conducted the numerical simulations and gathered the data. Both authors collaborated closely in analyzing the results, discussing their implications, and drawing conclusions. A. Benhamou provided valuable insights and expertise in computational fluid dynamics and structural analysis, contributing to the comprehensive understanding of the findings. The joint efforts of both authors, who also co-authored this article, ensured a thorough analysis of the results and the extraction of meaningful insights. S. M. Belghoula and A. Benhamou jointly reviewed and refined the interpretations, ensuring the accuracy and coherence of the conclusions presented in the manuscript.

REFERENCES

Adjiri, S., Dobrev, I., Benzaoui, A., Nedjari-Daaou, H., & Massouh, F. (2023). New Actuator Disk Model for the Analysis of Wind Turbines Wake Interaction with the Ground. *Journal of Applied Fluid Mechanics*, 16(1), 75-88. https://doi.org/10.47176/JAFM.16.01.1328

Agbormbai, J. T. (2021). *A vortex ring theory for horizontal-axis wind turbines and experimental investigation of the performance characteristics of a novel vertical-axis wind turbine* (Doctoral dissertation, University of Maryland]. Baltimore County). https://mdsoar.org/handle/11603/26039

Apsley, D. D., & Stansby, P. K. (2020). Unsteady thrust on an oscillating wind turbine: Comparison of blade-element momentum theory with actuator-line CFD. *Journal of Fluids and Structures*, 98, 103141. https://doi.org/10.1016/j.jfluidstructs.2020.103141

Bouhelal, A., Smaili, A., Guerri, O., & Masson, C. (2023). Numerical investigations on the fluid behavior in the near wake of an experimental wind turbine model in the presence of the nacelle. *Journal of Applied Fluid Mechanics*, 16(1), 21-33. https://doi.org/10.47176/jafm.16.01.1382

Casillas Farfán, C., Solorio Díaz, G., López Garza, V., Galván González, S., & Figueroa, K. (2022). Novel induction blade design for horizontal axis wind turbines to improve starting phase: Cfd and testing analysis. *Journal of Applied Fluid Mechanics*, 15(6), 1635-1648. https://doi.org/10.47176/JAFM.15.06.1163

Cheng, H., Lin, W. E. I., Bin, Z. H. O. U., Qiang, H. E., & Peng, X. I. A. O. (2017). Numerical study of lateral wind effect on parachute dropping based on finite element method. *Mechanics*, 23(1), 126-131. https://doi.org/10. 5755/J01.MECH.23.1.13679

Dahmane, M., Boutchicha, D., & Adjlout, L. (2016). One-way fluid structure interaction of pipe under flow with different boundary conditions. *Mechanics*, 22(6),495-503. https://doi.org/10.5755/J01.MECH.22.6.13189

de Langre, E. (2001). Simulation numérique en interaction fluide-structure. *La Houille Blanche*, (1), 34-38. https://doi.org/10.1051/lhb/2001005

Degroote, J. (2013). Partitioned simulation of fluid-structure interaction: Coupling black-box solvers with quasi-Newton techniques. *Archives of computational methods in engineering*, 20(3), 185-238. https://doi.org/10.1007/s11831-013-9085-5

Ebrahimi, E., Amini, Y., & Imani, G. (2021). Heat transfer characteristics of a circular cylinder covered by a porous layer undergoing vortex-induced vibration. *International Journal of Thermal Sciences*, 166, 106974. https://doi.org/10.1016/j.ijthermalsci.2021.106974

Gopalkrishnan, R. (1993). *Vortex-induced forces on oscillating bluff cylinders*. Woods Hole Oceanographic Institution MA. https://apps.dtic.mil/sti/citations/ADA265056

Hover, F. S., Techet, A. H., & Triantafyllou, M. S. (1998). Forces on oscillating uniform and tapered cylinders in cross flow. *Journal of Fluid Mechanics*, 363, 97-114. https://doi.org/10.1017/S0022112098001074

Hsu, M. C., & Bazilevs, Y. (2012). Fluid–structure interaction modeling of wind turbines: simulating the full machine. *Computational Mechanics*, 50, 821-833. https://doi.org/10.1007/s00466-012-0772-0

Lee, H. M., & Kwon, O. J. (2019). Numerical simulation of horizontal axis wind turbines with vortex generators. *International Journal of Aeronautical and Space Sciences*, 20, 325-334. https://doi.org/10.1007/s42405-018-0118-z

Lololau, A., Soemardi, T. P., Purnama, H., & Polit, O. (2021). Composite multiaxial mechanics: laminate design optimization of taper-less wind turbine blades with ramie fiber-reinforced polylactic acid. *International Journal of Technology*, 12(6), 1273-1287. https://doi.org/10.14716/ijtech.v12i6.5199

Mannion, B., Leen, S. B., & Nash, S. (2020). Development and assessment of a blade element momentum theory model for high solidity vertical axis tidal turbines. *Ocean Engineering*, 197, 106918. https://doi.org/10.1016/j.oceaneng.2020.106918

Mdouki, R. (2020). Parametric study of magnus wind turbine with spiral fins using bem approach. *Journal of Applied Fluid Mechanics*, 14(3), 887-895. https://doi.org/10.47176/JAFM.14.03.31789

Moghimi, M., & Motawej, H. (2020). Comparison aerodynamic performance and power fluctuation between darrieus straight-bladed and gorlov vertical axis wind turbines. *Journal of Applied Fluid Mechanics*, 13(5), 1623-1633. https://doi.org/10.36884/jafm.13.05.30833

Mohebbi, M., & Hashemi, M. (2017). Designing a 2-degree of freedom model of an unbalanced engine and reducing its vibrations by active control. *Civil Engineering*, 8(5). https://doi.org/10.14716/ijtech.v8i5.868

Năstase, E. V. (2021). Studies on the design models of horizontal axis wind turbines. *Bulletin of the Polytechnic Institute of Iași. Machine constructions Section*, 67(1), 9-18. https://doi.org/10.2478/bipcm-2021-0001

Panjwani, B., Popescu, M., Samseth, J., Meese, E., & Mahmoudi, J. (2014). *OffWindSolver: Wind farm design tool based on actuator line/actuator disk concept in OpenFoam architecture*. ITM Web of Conferences (Vol. 2, p. 04001). EDP Sciences. https://doi.org/10.1051/itmconf/20140204001

Sabino, D., Fabre, D., Leontini, J. S., & Jacono, D. L. (2020). Vortex-induced vibration prediction via an impedance criterion. *Journal of Mechanics*, 890, A4. https://doi.org/10.1017/jfm.2020.104

Sarpkaya, T. (2004). A critical review of the intrinsic nature of vortex-induced vibrations. *Journal of Fluids and Structures*, 19(4), 389-447. https://doi.org/10.1016/j.jfluidstructs.2004.02.005

Sayed, M., Lutz, T., Krämer, E., Shayegan, S., & Wüchner, R. (2019). Aeroelastic analysis of 10 MW wind turbine using CFD–CSD explicit FSI-coupling approach. *Journal of Fluids and Structures*, 87, 354-377. https://doi.org/10.1016/j.jfluidstructs.2019.03.023

Schaffarczyk, A. P., & Schaffarczyk, A. P. (2014). Application of Vortex Theory. *Introduction to Wind*

Turbine Aerodynamics, 99-119. https://doi.org/10.1007/978-3-642-36409-9_6

Scovazzi, G., & López Ortega, A. (2012). Algebraic flux correction and geometric conservation in ALE computations. *Flux-Corrected Transport: Principles, Algorithms, and Applications*, 299-343. https://doi.org/10.1007/978-94-007-4038-9_9

Sjah, J., & Vincens, E. (2017). Fluid–solid interaction in the case of piping erosion: validation of a SPH-ALE code. *International Journal of Technology*, 8(6), 1040-1049. https://doi.org/10.14716/ijtech.v8i6.729

Soti, A. K., & De, A. (2020). Vortex-induced vibrations of a confined circular cylinder for efficient flow power extraction. *Physics of Fluids*, 32(3), 033603. https://doi.org/10.1063/1.5131334

Takizawa, K., Spielman, T., Moorman, C., & Tezduyar, T. E. (2012). Fluid-structure interaction modeling of spacecraft parachutes for simulation-based design. *Journal of Applied Mechanics*, 79(1). https://doi.org/10.1115/1.4005070

Tang, D., Bao, S., Luo, L., Zhu, H., & Cui, H. (2019). A CFD/CSD coupled method with high order and its applications in flow induced vibrations of tube arrays in cross flow. *Annals of Nuclear Energy*, 130, 347-356. https://doi.org/10.1016/j.anucene.2019.03.003

Wu, Y., Lien, F. S., Yee, E., & Chen, G. (2023). Numerical investigation of flow-induced vibration for cylinder-plate assembly at low Reynolds number. *Fluids*, 8(4), 118. https://doi.org/10.3390/fluids8040118

Yang, Z., Yang, C., Zhao, J., & Wu, Z. (2022). Fluid–structure interaction dynamic response of rocket fairing in falling phase. *Aerospace*, 9(12), 741. https://doi.org/10.3390/aerospace9120741